Research Square

Preprints are preliminary reports that have not undergone peer review.
They should not be considered conclusive, used to inform clinical practice,
or referenced by the media as validated information.

Obstacle immune super resolution CMOS integrated THz imaging system based on a freeform caustic lens

Hao Guo

haoguo8@cityu.edu.hk

City University of Hong Kong https://orcid.org/0009-0005-7017-0499

Jin Chen

City University of Hong Kong https://orcid.org/0000-0001-9554-0445

Liang Gao

Southeast University

Zhi Chao Chen

City University of Hong Kong

Kang Jie Lin

Southeast University

Kam Man Shum

City Uiversity of Hong Kong https://orcid.org/0000-0002-8750-8581

Ka Fai Chan

City University of Hong Kong https://orcid.org/0000-0002-5719-6855

Chi Chan

City University of Hong Kong https://orcid.org/0000-0002-9718-0831

Article

Keywords:

Posted Date: November 18th, 2026

DOI: https://doi.org/10.21203/rs.3.rs-11356130/v1

License: This work is licensed under a Creative Commons Attribution 4.0 International License.
Read Full License

Additional Declarations: There is no conflict of interest

Obstacle-immune super-resolution CMOS-integrated THz imaging system based on a freeform caustic lens

Jin Chen[1#], Liang Gao[2#*], Hao Guo[1#*], Zhi Chao Chen,[1,3#] Kang Jie Lin[2], Kam Man Shum[1], Ka Fai Chan[1], Chi Hou Chan[1,4*]

[1] State Key Laboratory of THz and Millimeter Waves, City University of Hong Kong, Hong Kong, 999077, China

[2] School of Information Science and Engineering, State Key Laboratory of Millimeter Waves, Southeast University, Nanjing, 210096, China

[3] Institute of Plasma Physics, Chinese Academy of Sciences, Hefei, 230031, China

[4] Department of Electrical Engineering, City University of Hong Kong, Hong Kong, 999077, China

These authors contributed equally: Jin Chen, Liang Gao, Hao Guo, Zhi Chao Chen

[*]Corresponding author: lianggao@seu.edu.cn, haoguo8@cityu.edu.hk, eechic@cityu.edu.hk

Abstract

While terahertz (THz) radiation's ability to penetrate dielectrics holds great promise for non-destructive testing, opaque materials such as metals and large obstacles fundamentally limit this capability, particularly at higher frequencies. Endowing THz waves with obstacle-bypassing capabilities remains a formidable challenge for practical applications. Although conventional bottle beams can route energy around a central obstacle, their low spatial resolution precludes high-fidelity imaging of fine details. To address this, we propose an achromatic super-resolution bottle beam. Using caustic theory, we derive a phase profile that can theoretically circumvent a metallic disk obstacle with a 12 mm diameter and map it onto gradient-index (GRIN) and freeform lens designs. Here we report the experimental generation of a broadband super-resolution THz bottle beam spanning 0.5–1 THz, enabled by integrating a 3D-printed freeform lens with a compact 65-nm CMOS oscillator–radiator array. The beam features a sub-diffraction full width at half maximum (FWHM) of 0.8λ and a robust 4-mm depth of focus. This integrated system achieves high-precision recognition of sub-millimeter features (down to 0.2mm) in complex targets, such as USAF 1951 charts and a biomimetic network structure resembling biological tissues. Crucially, the super-resolution imaging performance is flawlessly maintained even in the presence of the 12-mm metal disk. Furthermore, volumetric 3D imaging through highly scattering media is also validated. Our work establishes a robust paradigm, highlighting the transformative potential of super-resolution bottle beams in complex non-destructive imaging scenarios.

Introduction

Owing to its penetrative and non-ionizing nature, terahertz (THz) radiation has emerged as a highly promising modality for numerous applications, including the detection of explosives and illicit drugs[1-2], authentication of artworks and antiques[3-4], and pharmaceutical quality control[5-7]. However, in practical scenarios, this intrinsic

penetrative capability is fundamentally hindered by macroscopic obstacles or opaque metallic objects. Consequently, developing THz imaging and sensing techniques with robust obstacle-circumventing capabilities is paramount.

Cylindrically symmetric Airy beams, commonly known as abrupt autofocusing (AAF) beams[8-10], offer a compelling paradigm to overcome this limitation. During propagation, an AAF beam initially forms a hollow intensity profile featuring a dominant annular main lobe and weaker concentric sidelobes. This central dark void inherently provides a physical pathway to bypass obstacles. Further along the propagation axis, the beam abruptly converges into a high-intensity focal spot. The resulting focused field exhibits a pseudo-Bessel profile, with a highly localized central lobe surrounded by faint annular sidelobes—ideal for high-resolution THz imaging and communications. To date, researchers have harnessed the unique propagation dynamics of AAF beams for diverse applications, such as obstacle-immune microwave wireless power transfer[11], high-resolution confocal fluorescence microscopy[12], precise laser surgery[13], and optical trapping[14]. Despite these cross-disciplinary successes, the AAF beams in the THz regime remain largely unexplored.

Moreover, because THz wavelengths are macroscopically larger than their optical counterparts, super-resolution strategies are essential for achieving high-performance imaging. However, the intrinsically low numerical aperture (NA) of AAF beams substantially degrades their resolving capability. This limitation is further compounded by the absence of a systematic evaluation of key imaging metrics, including FWHM and focusing efficiency. Consequently, conventional AAF beams are intrinsically unsuitable as an effective platform for super-resolution, obstacle-avoiding THz imaging.

Bottle beams, an alternative class of hollow beams originally generated via computer-generated holograms[15], emerge as a prime candidate[16] for achieving obstacle-immune, super-resolution THz imaging. Although previous research on bottle beams has predominantly focused on optical tweezers[17] and trapping [18-21], caustic theory offers a highly promising pathway to get the desired bottle beams. Governed by the principles of geometric optics, caustic theory predicts a dynamic propagation in which a hollow dark region seamlessly transitions into a tight focal spot. The corresponding phase profile is implemented via metasurfaces [22] to achieve basic obstacle-avoidance focusing. Unfortunately, rigorous assessments of focusing performance and subsequent investigations into functional applications remain unexplored. Moreover, although high-NA metasurfaces with large apertures are essential for obstacle-avoiding super-resolution imaging, the application is severely hampered by limited operational bandwidth and pronounced chromatic aberrations.

Alternatively, building upon the phase-engineering principles established in our previous work on aberration-free metalenses[23], gradient-index (GRIN) lenses emerge as a compelling platform for generating achromatic, super-resolution bottle beams with high-fidelity THz imaging capabilities. Theoretically, the targeted phase profile can be accurately mapped onto a volumetric GRIN distribution of a finite thickness. However, current manufacturing technologies impede practical implementations. Specifically, fabricating large-aperture THz GRIN lenses, strictly required for effective obstacle circumvention, poses prohibitive technological challenges. Therefore, the experimental

realization of super-resolution, obstacle-immune THz imaging remains a critical bottleneck in the field.

In this work, we derive a prescribed phase profile from caustic theory to generate a super-resolution bottle beam that integrates obstacle-circumventing capability with an extended depth of focus (DOF). To mitigate the severe chromatic aberrations and limited operational bandwidths inherent to conventional metasurface implementations, we further mathematically map this phase profile, inspired by our previous lens architectures[24], onto an equivalent GRIN distribution and freeform surface. Subsequently, the proposed freeform lens is manufactured by high-precision 3D printing. Both theoretical modeling and experimental characterization confirm that the device provides robust achromatic focusing across 0.5 to 1 THz. Notably, it maintains a sub-diffraction FWHM of ~0.8λ alongside an extended DOF of ~10λ. Translating these advanced optical capabilities into a practical system, we constructed a compact, obstacle-immune 3D THz imaging platform by integrating the freeform lens with a 65-nm CMOS-based oscillator-radiator array[25] (Fig. 1). Experimental evaluations reveal that sub-millimeter features with a strict 0.2-mm pitch—such as those within USAF 1951 targets and intricate bioinspired patterns—are resolved with outstanding faithfulness. Notably, as theoretically anticipated, this super-resolution performance is robustly preserved even when obstructed by a macroscopic 12-mm metal obstacle. Furthermore, volumetric 3D imaging is also realized through scattering media. Overall, our work establishes a versatile framework for engineering bottle beams, providing a route towards high-resolution non-destructive testing in complex environments and opening opportunities for transformative applications across diverse fields.

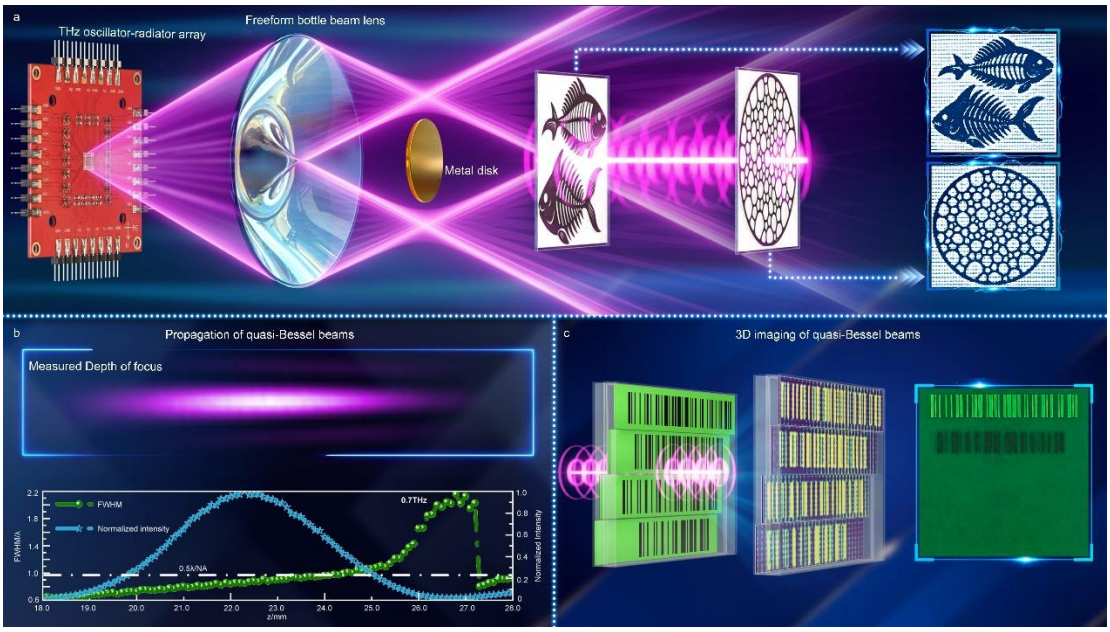


Fig. 1. An obstacle-immune super-resolution THz imaging system realized by a freeform caustic lens and a THz oscillator-radiator array. a. Integrated THz obstacle-immune super-resolution imaging system**. b.** Quasi-Bessel beam propagation with an extended depth of focus. **c**. 3D imaging results of quasi-Bessel beam.

Results

Theoretical design of THz freeform caustic lens

To derive the targeted phase profile for the super-resolution bottle beam within the framework of caustic theory, we employ a two-dimensional (2D) geometric ray-tracing analysis. To facilitate the analytical derivation, the central intensity void is geometrically modeled as a circle, as illustrated in Fig. 1b. The corresponding analytical expression is given by:

$$f(z) = \pm\sqrt{r_0^2 - (z - r_0)^2} \tag{1}$$

where r_0 denotes the radius of the central dark region. Given that ray trajectories geometrically constitute a family of tangent lines enveloping this circular boundary, the targeted phase profile can be derived by applying the generalized law of refraction[25-26], yielding the following expression:

$$\frac{\mathrm{d}\varphi(x)}{\mathrm{d}x} = -k\sin\theta \tag{2}$$

where k is the vacuum wavenumber, and θ denotes the angle of the tangent ray. By defining (x_0, z_0) as the tangent point on the circle and (x_1,0) as its intercept on the x-axis, the geometric slope satisfies tanθ = -df(z)/dz. Consequently, x_1 is analytically given by:

$$x_1 = f(z_0) - z_0 f'(z_0) \tag{3}$$

The simultaneous solutions of Eqs. (1), (2), and (3) yield the targeted phase profile, given by:

$$\varphi(x) = \pi - k\left[|x| - 2r_0\, arctan\left(\frac{|x|}{r_0}\right)\right] \tag{4}$$

Owing to the cylindrical symmetry, the 2D phase profile could be expressed as:

$$\varphi(r) = \pi - k\left[r - 2r_0\, arctan\left(\frac{r}{r_0}\right)\right] \tag{5}$$

To optimize the optical performance, the radii of the phase plate (R) and the central dark region (r_0) were set to 14 mm and 6 mm, respectively. Subsequently, the derived 2D phase profile is transformed into the equivalent GRIN distribution:

$$n(r) = 1 - 0.2r + 2.4\arctan(\frac{r}{6}) \tag{6}$$

Ultimately, the GRIN lens described by Equation 6 with a thickness of 5 mm is translated into the corresponding freeform lens as shown in Fig. 2a. The details of this transformation are given in Supplementary Note 1. The calculated ray tracing and electric field distributions at 0.7 THz of three kinds of bottle beam lenses are illustrated in Fig. 2b-c, indicating that the equivalence between metasurface, GRIN lens, and freeform lens is effective. To further validate the focusing performance across the entire

frequency range from 0.5 THz to 1 THz quantitatively, the corresponding electric field distributions in the *x*-*z* plane and *x*-*y* plane were rigorously calculated and depicted in Figs. S2 and S3, respectively. Ultra-broadband, achromatic, and obstacle-resilient focusing spanning 0.5–1.0 THz with an extended DOF exceeding 10λ is achieved by the proposed freeform caustic lens. The extracted focusing resolution and efficiency—summarized in Fig. 3 b-c—demonstrate high-efficiency (~60%) obstacle-resilient focusing characterized by an FWHM of approximately 0.8λ. The extended DOF (>10λ) enabled by this freeform architecture is detailed in Fig. S3b. Furthermore, the axial evolution of the FWHM alongside the intensity profile of the THz needle is quantitatively evaluated in Fig. 2d. Crucially, the FWHM remains sub-diffraction-limited, consistently bounded below 0.5λ/NA across the entire DOF. This robust longitudinal confinement underlines the substantial utility of the freeform caustic lens for high-fidelity, obstacle-tolerant 3D volumetric imaging.

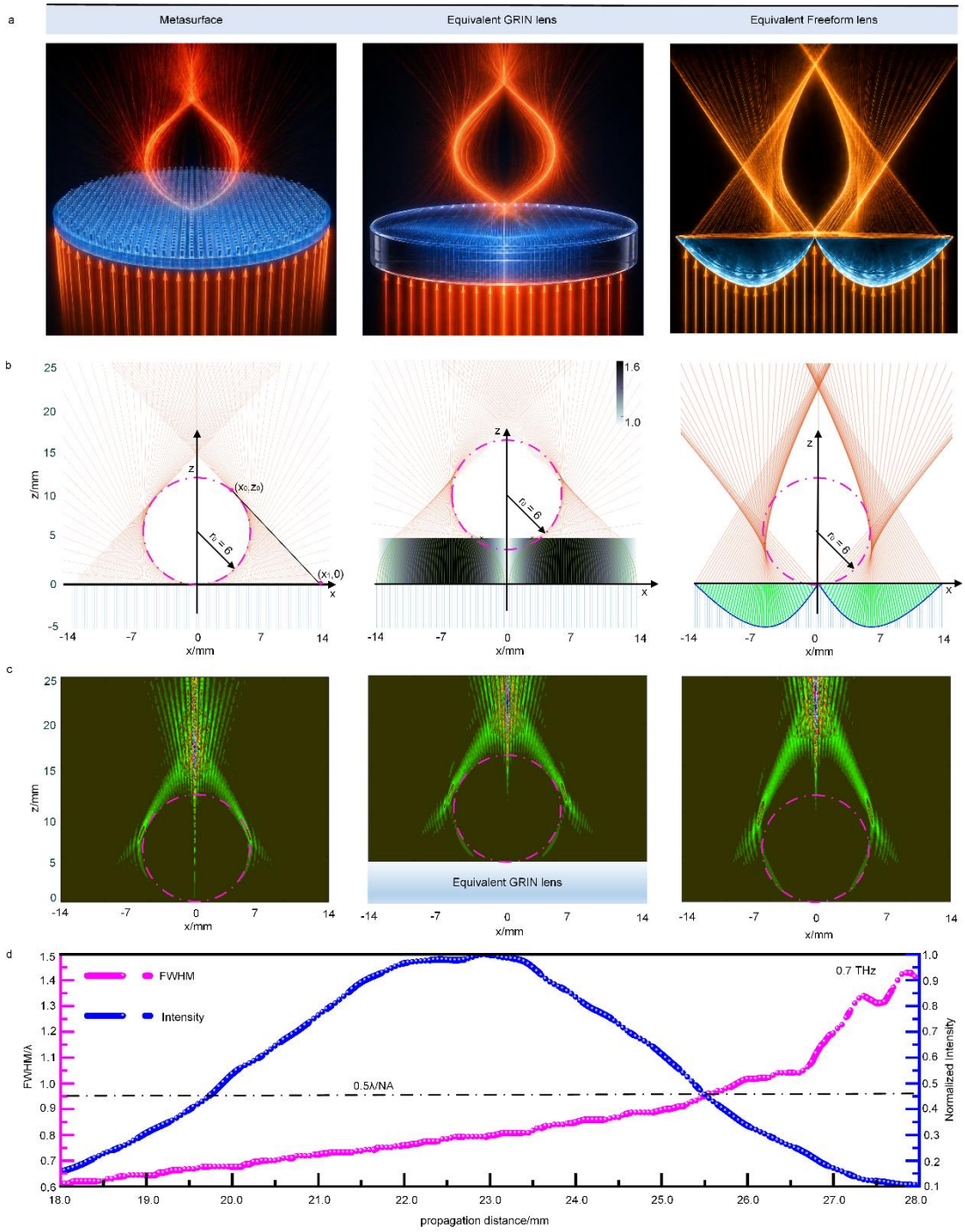


Fig. 2. Theoretical design of an obstacle-immune freeform caustic lens. **a.** Evolution of bottle beam lens from metasurface to freeform caustic lens. **b-c**. Calculated ray tracing and electric field distributions at 0.7 THz for three types of bottle-beam lenses. **d**. FWHM and intensity of the THz needle's main lobe along the propagation direction at 0.7 THz.

Experimental demonstration of the proposed THz freeform caustic lens

A dedicated measurement platform was constructed to capture the electric-field distributions and to assess the achromatic focusing response, as illustrated in Fig. S4. The experimentally recorded intensity maps in both the *x*–*z* and *x*–*y* planes, shown in Fig. 3a, clearly verify broadband achromatic focusing throughout the 0.5–1.0 THz spectral window. The corresponding normalized field patterns at the focal planes further

reveal the focusing characteristics across the band. As summarized in Fig. 3b, the measured FWHM and focusing efficiency remain nearly invariant at approximately 0.8λ and 60%, respectively, in close agreement with theoretical expectations; the small discrepancies observed can be attributed to standard experimental tolerances.

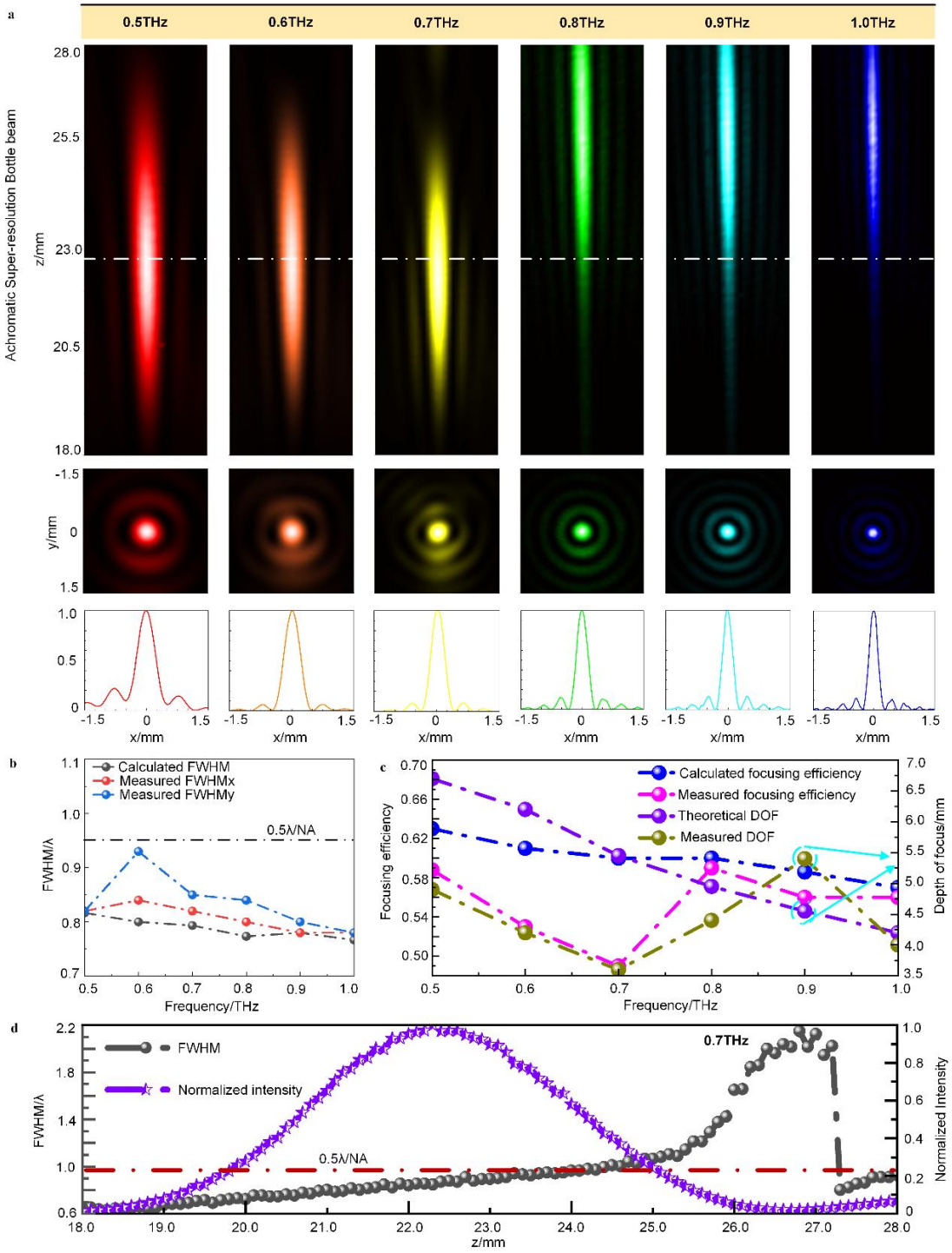


Fig. 3 Experimental results of achromatic focusing with an extended depth of focus. a. Experimentally recorded electric-field maps in the x–z and x–y planes over 0.5–1.0 THz, together with the corresponding field profiles extracted along the focal line. **b-c**. Experimental and theoretical comparisons of the FWHM, DOF, and focusing efficiency. **d**. Evolution of the measured FWHM and main-lobe intensity of the THz needle beam along the propagation axis at 0.7 THz.

The intrinsic dispersion of the resin[24] introduces a frequency dependence in the focal position, with the focal length increasing gradually as the incident frequency increases (Fig. 3a). Material dispersion also contributes to the discrepancy between the simulated and measured DOF, with the measured DOF remaining approximately 4.0–5.0 mm (Fig. 3d). Figure 3d further presents the measured axial profiles of the beam's FWHM and on-axis intensity. The FWHM remains below 0.5λ/NA throughout the effective DOF, where λ is the free-space wavelength, and NA is the numerical aperture. Despite material dispersion, the combination of a narrow transverse beam profile and an extended axial focal region highlights the potential of the 3D-printed freeform caustic lens for high-resolution volumetric THz imaging.

A compact THz imaging system of a freeform caustic lens and an oscillator–radiator array

By combining the designed freeform caustic lens with the oscillator–radiator array, we constructed a compact terahertz imaging platform, as illustrated in Fig. S5. The array emits y-polarized radiation at 0.658 THz, and the freeform caustic lens converts it into an obstacle-immune beam with an extended DOF for sample illumination. Finally, a receiving probe collected the transmitted THz signals. For 2D imaging, the target is mounted on a motorized translation stage and continuously scanned in the x–y plane; the acquired intensity signals are then computationally processed to reconstruct the images.

To evaluate the imaging performance under demanding conditions, we used a USAF 1951 resolution target and biomimetic network structures resembling biological tissues, such as fish and leaf cells, each containing features as small as 0.2 mm. These samples provide stringent tests of image fidelity, since the sidelobes inherent to caustic beams can otherwise generate artifacts and compromise the resolution of complex structures. Biomimetic network-patterned specimens for imaging were fabricated by lithographically patterning the target structures in the internal layer of a thin printed circuit board, as shown in the optical micrograph in Fig. S6.

Although residual background artifacts are obvious in the raw reconstructions, the fine features of the USAF 1951 resolution target and the embedded biomimetic network patterns remain clearly discernible, as presented in Fig. S7. To further attenuate these artifacts and enhance image fidelity, we implemented a tailored computational refinement workflow that integrates deconvolution, stripe-noise suppression, and axial constraint filtering[25]. As shown in Fig. 4a–c, this treatment effectively suppresses spurious background contributions, thereby substantially improving image clarity. The resulting images display significantly enhanced contrast relative to the unprocessed measurements. The proposed miniaturized THz imaging system resolves features as small as 0.15 mm in a USAF 1951 resolution target and reliably distinguishes 0.2-mm features in complex patterns.

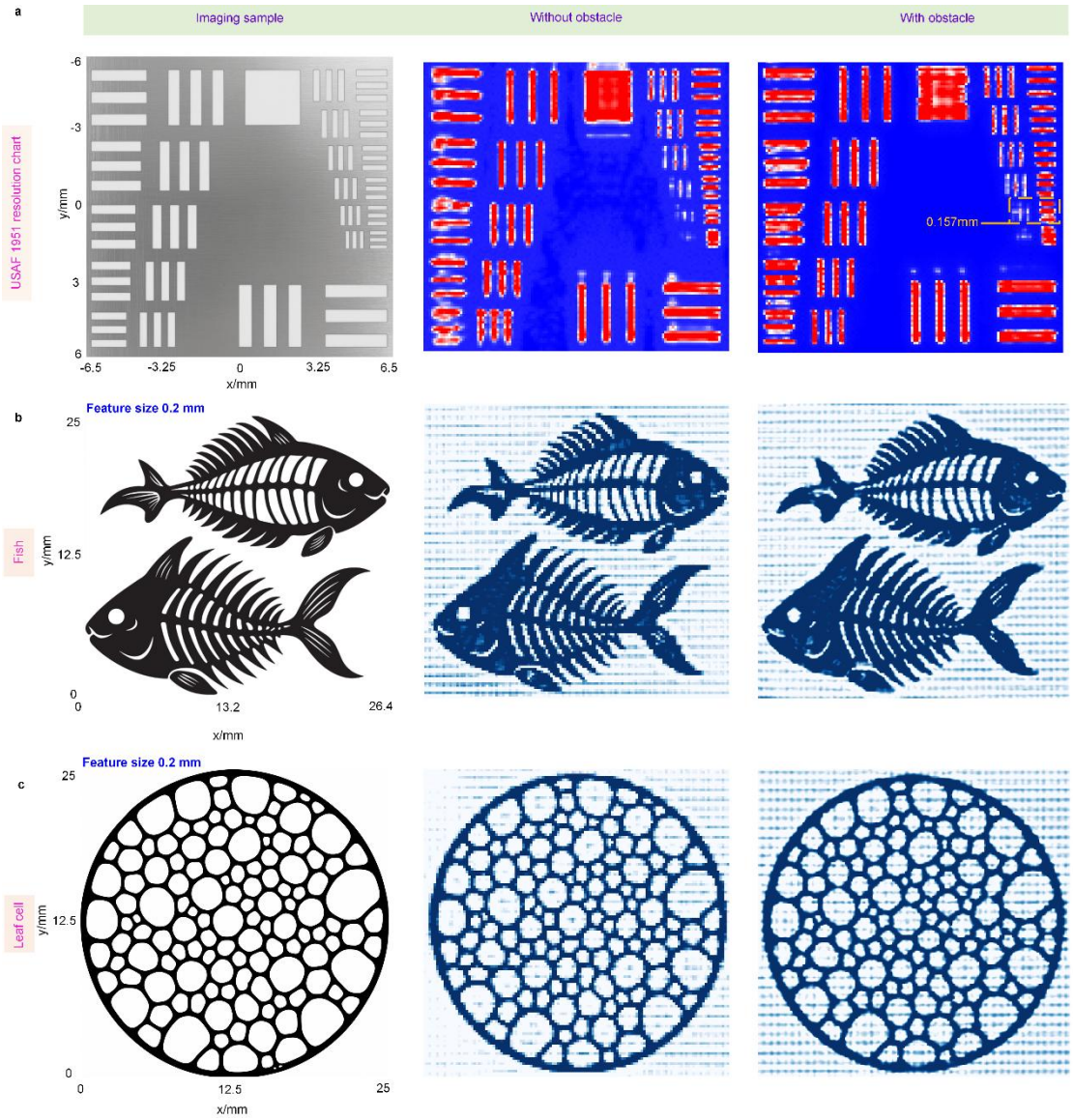


Fig. 5. **Imaging results of the obstacle-immune super-resolution CMOS-integrated THz imaging system. a-c**. Imaging samples comprising a USAF 1951 resolution target and fish and leaf cell patterns with 0.2-mm features, together with the corresponding images acquired with and without intervening obstacles.

The overlapping and intersecting caustic trajectories downstream of the designed lens produce a beam structure reminiscent of a Bessel beam. This similarity motivates an investigation of the beam's self-healing behavior and its potential for depth-resolved imaging within scattering media, such as PCB substrates. To further evaluate the 3D imaging capability of the developed THz system, barcodes encoding the text strings "CityUHK," "SKLMTW," "ABCD," and "AB," each with a minimum bar width of 0.2 mm ("CityUHK" and "SKLMTW") and 0.3mm ("ABCD" and "AB"), were embedded at distinct axial depths within a 1.5-mm-thick PCB substrate. Fig. 6a shows an optical photograph of the multilayer PCB substrate, and Fig. 6b presents a perspective schematic illustrating its 3D layout. The original patterns of these 4 barcodes are listed in Fig. 6c. The imaging result of the 4 barcodes is illustrated in Fig. 6d. It can be observed that most details of the embedded barcodes are recovered successfully. The

self-healing property of our designed bottle beam is ultimately demonstrated.

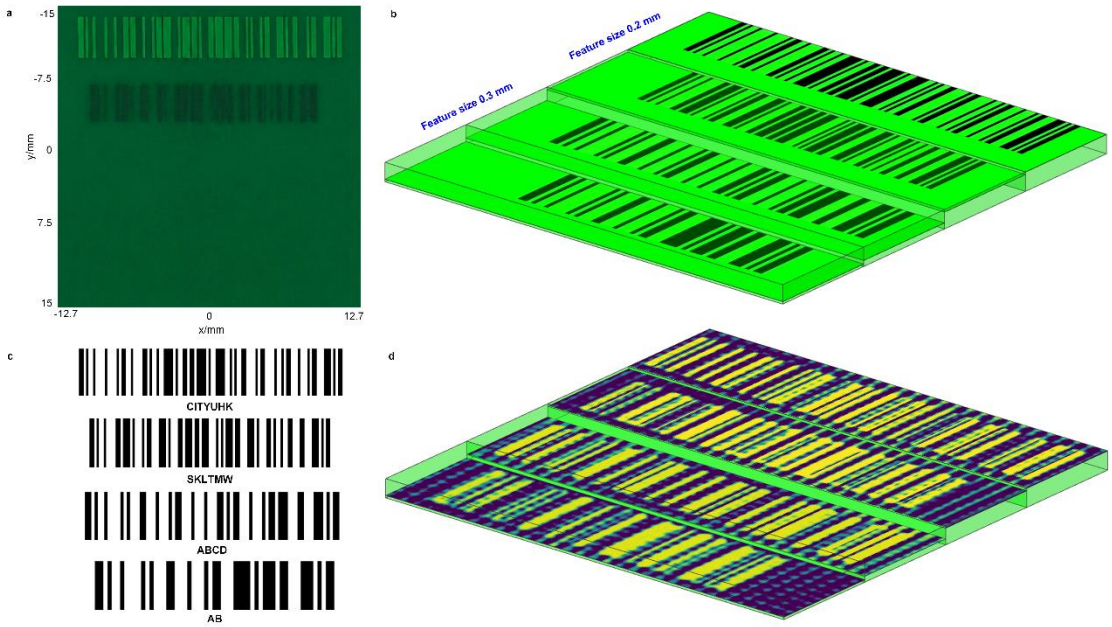


Fig. 6. **Multi-layer PCB and the corresponding imaging results. a**. Optical Image of the PCB with 4 barcodes embedded. **b.** 3D geometric layout of the multi-layered PCB substrate. **c.** Original patterns of the 4 barcodes. **d.** Imaging results of the 4 barcodes within the PCB.

Discussion

In conclusion, we have developed a broadband THz imaging framework that simultaneously enables sub-diffraction spatial resolution, an extended depth of focus, and robust operation in the presence of macroscopic opaque obstacles. By employing caustic theory to engineer the desired wavefront, the terahertz field is guided around a central obstruction and subsequently reconstructed into a tightly confined focal region. To circumvent the pronounced chromatic dispersion associated with conventional metasurface implementations, the prescribed phase distribution is translated into equivalent gradient-index and freeform optical geometries. The resulting freeform lens, fabricated using inexpensive additive manufacturing, is integrated with a compact oscillator–radiator array implemented in 65-nm CMOS technology. Electric-field measurements confirm achromatic focusing across 0.5–1 THz, yielding a transverse FWHM of approximately 0.8 λ and a depth of focus approaching 4 mm, corresponding to approximately 10 λ. The integrated platform resolves features with a pitch as small as 0.15 mm in standard resolution targets and achieves a spatial resolution of 0.2 mm in biologically inspired network structures. Notably, this imaging fidelity is preserved even when a metallic obstacle (12 mm in diameter) blocks the direct propagation path, validating the beam's robust field-reconstruction and obstacle-bypassing capabilities. Volumetric imaging through highly scattering media is further demonstrated. These results establish a practical and scalable route toward broadband THz wavefront engineering and may facilitate high-resolution, 3D nondestructive inspection in obstructed, scattering, and otherwise challenging environments.

Data availability

The data that support the findings of this study are presented in the paper and the Supplementary Information file.

Reference

[1] A. G. Davies, A. D. Burnett, W. H. Fan, E. H. Linfield, J. E. Cunningham, Terahertz spectroscopy of explosives and drugs. Mater. Today. 11, 18-26 (2008)

[2] J. F. Federici, B. Schulkin, F. Huang, D. Gary, R. Barat, F. Oliveria, D. Zimdars, THz imaging and sensing for security applications—explosives, weapons and drugs. Semicond. Sci. Technol. 20, S266–S280 (2005)

[3] C. Seco-Martorell, V. Lopez-Dominguez, G. Arauz-Garofalo, A. Redo-Sanchez, J. Palacios, J. Tejada, Goya's artwork imaging with Terahertz waves. Opt. Express. 21, 17800-17805 (2013)

[4] Y. Q. Cui, Y. F. Xu, D. H. Han, X. Y. Wang, Z. L. Shen, Y. H. Hou, J. Y. Liang, X. Q. Wang, D. S. Citrin, L. Y. Zhang, A. K. Nandi, R. Q. Yan, X. F. Chen, Hidden-information extraction from layered structures through terahertz imaging down to ultralow SNR. Sci. Adv. 9, eadg8435 (2023)

[5] A. Moradikouchi, A. Sparen, O. Svensson, S. Folestad, J. Stake, H. Rodilla, Terahertz frequency-domain sensing combined with quantitative multivariate analysis for pharmaceutical tablet inspection, Int. J. Pharm 632, 122545 (2023)

[6] H. Q. Wu, M. Khan, THz spectroscopy: An emerging technology for pharmaceutical development and pharmaceutical Process Analytical Technology (PAT) applications, J. Mol. Struct 1020, 112-120 (2012)

[7] D. Markl, M. T. Ruggiero, J. A. Zeitler, Pharmaceutical applications of terahertz spectroscopy and imaging. Eur. Pharm. Rev 21, 45-50 (2016).

[8] D. G. Papazoglou, N. K. Efremidis, D. N. Christodoulides, and S. Tzortzakis, Observation of Abruptly Autofocusing Waves, Opt. Lett 36, 1842–1844 (2011)

[9] N. K. Efremidis and D. N. Christodoulides, Abruptly Autofocusing Waves, Opt. Lett 35, 4045–4047 (2010)

[10] I. Chremmos, N. K. Efremidis, D. N. Christodoulides, Pre-engineered abruptly autofocusing beams, Opt. Lett 36, 1890–1892 (2011)

[11] S. Zhang, H. Xue, Z. Zheng, X. J. Ma, X. Wang, J. Q. Han, H. X. Liu, L. Ki, Obstacle-Immune Microwave Wireless Power Transfer System Based on Amplitude-Dependent Caustic Metasurface, Adv. Sci. 12, e10070 (2025)

[12] Y. Luo, S. A. Suresh, S. Vyas, C. H. Chu, W-H. Liao, W-S. Chen, J. A. Yeh, D. P. Tasi, P-C. Yang, Abrupt Autofocusing Metasurface for High-Resolution Confocal Fluorescence Microscopy, Laser Photon. Rev 20, e01798 (2026)

[13] Y. Luo, M. L. Tseng, S. Vyas, H. Y. Kuo, C. H. Chu, M. K. Chen, H-C. Lee, W-P. Chen, V-C. Su, X. Shi, H. Misawa, D. P. Tsai, P-C. Yang, Metasurface-Based Abrupt Autofocusing Beam for Biomedical Applications, Small Methods 6, 2101228 (2022)

[14] F. X. Lu, H. Wu, Y. Lang, L. Tan, Z. F. Tan, X. Feng, Y. Hu, Y. X. Xiang, X. B. H, Z. G. Chen, J. J. Xu, Bessel-modulated autofocusing beams for optimal trapping implementation. Phys. Rev. A 104, 043524 (2021)

[15] J. Arlt, M. J. Padgett, Generation of a beam with a dark focus surrounded by regions of higher intensity: the optical bottle beam, Opt. Lett 25, 191–193 (2000)

[16] P. Genevet, J. Dellinger, R. Blanchard, A. She, M. Petit, B. Cluzel, M. A. Kats, F. Fornel, F.

Capasso, Generation of two-dimensional plasmonic bottle beams, Opt. Express 21, 110295-10300 (2013)
[17] S. K. Mondal, S. S. Pal, P. Kapur, Optical fiber nano-tip and 3D bottle beam as non-plasmonic optical tweezers, Opt. Express 20, 16180-16185 (2012)
[18] D. Barredo, V. Lienhard, P. Scholl, S. Leseleuc, T. Boulier, A. Browaeys, T. Lahaye, Three-Dimensional Trapping of Individual Rydberg Atoms in Ponderomotive Bottle Beam Traps. Phys. Rev. Lett. 124, 0023021(2020)
[19] Y. Z. Xiao, Z. N. Yu, R. A. Wambold, H. Y. Mei, G. Hickman, R. H. Goldsmith, M. Saffman, M. A. Kats, Efficient generation of optical bottle beams, Nanophotonics 10, 2893-2901 (2021)
[20] L. Isenhower, W. Williams, A. Dally, M. Saffman, Atom trapping in an interferometrically generated bottle beam trap, Opt. Lett 34, 1159-1161 (2009)
[21] G. Li, S. Zhang, L. Isenhower, K. Maller, M. Saffman, Crossed vortex bottle beam trap for single-atom qubits, Opt. Lett 37, 851-853 (2012)
[22] M. L. Lin, B. Ratni, P. H. Qi, J. J. Yi, A. D. Lustrac, S. N. Burokur, Flexible Generation and Manipulation of Microwave Bottle Beam Using a Reconfigurable Metamirror, Adv. Photon. Res. **4**, 2300156 (2023)
[23] J. Chen, S. H. Huang, K. F. Chan, G. B. Wu, and C. H. Chan. 3D-printed aberration-free terahertz metalens for ultra-broadband achromatic super-resolution wide-angle imaging with high numerical aperture. Nat Commun 16, 363 (2025)
[24] J. Chen, S. H. Huang, K. F. Chan, G. B. Wu, H. Wong, and C. H. Chan. The Equivalence of Microlens and Metalens for THz High Spatial-Spectral Resolution Hyperspectral Imaging with a Large Field of View. Adv. Optical Mater. 13, e02943 (2025)
[25] J. Chen, L. Gao, H. Guo, Z. C. Chen, K. J. Lin, K. M. Shum, K. F. Chan, and C. H. Chan. An integrated super-resolution THz 3D imaging system based on a linear nonlocal achromatic freeform Bessel beam lens and high-power oscillator–radiator array. Preprint at https://doi.org/10.48550/arXiv.2607.19652 (2026)

Acknowledgments

This research was supported in part by the Research Grants Council of Hong Kong under the General Research Fund (grant CityU 11214123).

Author information

These authors contributed equally: Jin Chen, Liang Gao, Hao Guo, Zhi Chao Chen

Authors and affiliations.

State Key Laboratory of THz and Millimeter Waves, City University of Hong Kong, Hong Kong, 999077, China
Jin Chen, Hao Guo, Zhi Chao Chen, Kam Man Shum, Ka Fai Chan, & Chi Hou Chan

School of Information Science and Engineering, State Key Laboratory of Millimeter Waves, Southeast University, Nanjing, 210096, China
Liang Gao, Kang Jie Lin

Institute of Plasma Physics, Chinese Academy of Sciences, Hefei, Anhui 230031, China
Zhi Chao Chen

Department of Electrical Engineering, City University of Hong Kong, Hong Kong, 999077, China

Chi Hou Chan

Contributions

C.H.C., L. G, and H. G initiated the plan and supervised the entire study. C.H.C. and J.C. conceived the idea of this work. J. C. carried out the lens design and implemented the theoretical analysis. L. G designed the THz radiator array. H. G and K. J. L. completed the testing of the THz radiator array. J.C., H.G., K.S.M., and K.F.C. designed the experimental setup. J.C. and H.G. performed the imaging experiments. Z. C. C. performed the post-processing of the original imaging data. J.C. analysed the data and prepared the manuscript with input from all authors. C.H.C., L. G and H. G reviewed and edited the manuscript.

Corresponding author

Correspondence to Liang Gao, Hao Guo, and Chi Hou Chan.

Ethics declarations

Competing interests

The authors declare no competing interests.

Supplementary Files

This is a list of supplementary files associated with this preprint. Click to download.

- Supplementary2.docx